

Parametric Mapping of Binding in Human Brain of D₂ Receptor Ligands of Different Affinities

Thomas Siessmeier, MD¹; Yun Zhou, PhD²; Hans-Georg Buchholz, MSc¹; Christian Landvogt, MD¹; Ingo Vernaleken, MD³; Markus Piel, PhD⁴; Ralf Schirmmayer, PhD¹; Frank Rösch, PhD⁴; Mathias Schreckenberger, MD¹; Dean F. Wong, MD, PhD²; Paul Cumming, PhD⁵; Gerhard Gründer, MD⁶; and Peter Bartenstein, MD¹

¹Department of Nuclear Medicine, University of Mainz, Mainz, Germany; ²Division of Nuclear Medicine, Department of Radiology, Johns Hopkins Medical Institutions, Baltimore, Maryland; ³Department of Psychiatry, University of Mainz, Mainz, Germany; ⁴Institute for Nuclear Chemistry, University of Mainz, Mainz, Germany; ⁵PET Center and Center for Functionally Integrative Neuroscience, Aarhus, Denmark; and ⁶Department of Psychiatry and Psychotherapy, RWTH Aachen University, Aachen, Germany

¹¹C-Raclopride has been widely used for PET studies of dopamine D_{2/3} receptors in human brain. The long half-life of ¹⁸F may impart advantages to the novel moderate-affinity benzamide ¹⁸F-desmethoxyfallypride and its high-affinity congener ¹⁸F-fallypride for competition studies and for detection of extrastriatal binding. However, the in vivo kinetics of these compounds and the quantification approaches for parametric mapping of their specific bindings have not been systematically compared.

Methods: Dynamic emission recordings of the 3 tracers were obtained in groups of healthy subjects. A conventional model, graphical analysis using metabolite-corrected arterial inputs, and models with reference tissue inputs were used to calculate voxelwise parametric maps of the equilibrium distribution volume (V_d) and the binding potential (BP) of the 3 radioligands in brain. To test for bias, voxelwise kinetic results were compared with those obtained by volume-of-interest (VOI) analysis. **Results:** The V_d and BP estimates obtained by VOI analysis did not differ from the mean of voxelwise estimates in the same striatal volumes. In striatum, the mean ¹⁸F-desmethoxyfallypride BP ranged from 1.9 to 2.5, whereas the mean ¹¹C-raclopride BP ranged from 3 to 4, depending on the method used for calculation. In contrast, the mean BP of ¹⁸F-fallypride ranged from 16 to 27 in striatum and could also be readily quantified in the thalamus. **Conclusion:** Reference tissue methods for the voxelwise calculation of binding parameters are suitable for parametric mapping of the 3 dopamine D_{2/3} receptor ligands.

Key Words: fallypride; raclopride; desmethoxyfallypride; quantification; binding potential; parametric

J Nucl Med 2005; 46:964–972

The relative concentration in brain of dopamine D_{2/3} receptors has been assessed in PET studies of normal volunteers and in pathophysiologic conditions such as move-

ment disorders (1), schizophrenia (2,3), and alcoholism (4). Most PET studies assessing dopamine D_{2/3} receptor densities have used the reversibly binding and highly selective dopamine D_{2/3} benzamide antagonist ¹¹C-raclopride (¹¹C-RAC) (5–7). However, the short physical half-life of ¹¹C (20 min) imposes the requirement for an on-site medical cyclotron and, furthermore, entails certain practical limitations to the use of ¹¹C-RAC. In particular, ¹¹C-RAC may not be an optimal radiotracer for pharmacologic challenge studies in which binding is perturbed after equilibrium has been attained. For these reasons, Mukherjee et al. (8) developed benzamide ligands labeled with ¹⁸F-fluorine, which has a physical half-life of 110 min. Among these ligands, ¹⁸F-desmethoxyfallypride ((S)-N-[(1-allyl)-2-pyrrolidinylmethyl]-5-(3-¹⁸F-fluoropropyl)-2-methoxybenzamide) (¹⁸F-DMFP) has similar in vivo affinity and selectivity to ¹¹C-RAC (9), whereas ¹⁸F-fallypride ((N-[(1-allyl)-2-pyrrolidinylmethyl]-5-(3-¹⁸F-fluoropropyl)-2,3-dimethoxybenzamide) (¹⁸F-FP) is a high-affinity ligand suitable for the quantification of extrastriatal D_{2/3} receptor binding (10). Both tracers can be prepared with ¹⁸F generated at an off-site cyclotron unit. The relatively long retention of both ligands at the D_{2/3} receptor site combined with the long physical half-life may favor the use of these tracers in pharmacologic challenge studies (10).

Diverse methods for the quantification of ¹¹C-RAC binding in living brain have been reported (5,11–15). These methods include relatively invasive techniques requiring a metabolite-corrected arterial input function and more convenient techniques using a nonbinding reference tissue or simple binding ratios. The choice of method can influence the trade-off between precision and accuracy in the estimation of binding potential (BP), the parameter of interest, which is proportional to the density of dopamine receptors, reduced to some extent by competition from endogenous dopamine. Parametric mapping of receptor BP is useful for statistical comparisons of different populations and correlation to external covariates such as clinical rating, without

Received Oct. 19, 2004; revision accepted Feb. 14, 2005.

For correspondence or reprints contact: Thomas Siessmeier MD, Department of Nuclear Medicine, University of Mainz, Langenbeckstrasse 1, 55131 Mainz, Germany.

E-mail: siessmeier@nuklear.klinik.uni-mainz.de

a priori hypotheses about the anatomic locus of such correlations (4,16,17). Several of the methods developed for ^{11}C -RAC analysis are suitable for the voxelwise calculation of BP maps, allowing for the undirected search for altered patterns of $\text{D}_{2/3}$ receptor availability (7).

In contrast to ^{11}C -RAC, ^{18}F -DMFP and ^{18}F -FP are relatively new radiopharmaceuticals with distinct pharmacokinetic properties in vivo. There has been no systematic comparison of results of the several possible methods for the voxelwise quantification of the binding of these 3 tracers in human brain. The purpose of this study was therefore to compare the results of different methods suitable for voxelwise parametric mapping of ^{11}C -RAC, ^{18}F -DMFP, and ^{18}F -FP to provide the basis for selection of standard methods for planned clinical investigations. Therefore, a conventional standard 2-tissue-compartment model with metabolite-corrected arterial input was used to estimate the distribution volume (V_d) and BP of the 3 ligands in groups of healthy volunteers (11,18). Several voxelwise mapping procedures were tested, including reference tissue and arterial input methods. Finally, results of the voxelwise mapping were compared with volume-of-interest (VOI) analysis to test for bias.

MATERIALS AND METHODS

The study was approved by the local institutional ethics committees and the national radiation safety authorities. All volunteers were examined to exclude psychiatric, neurologic, or other diseases and were screened for substance abuse; they gave written, informed consent before the investigation. Before undergoing PET, T1-weighted MR head images had been obtained from each subject using a 1.5-T magnet (Siemens Vision). Intravenous catheters were placed in the antecubital vein of the dominant arm and the radial artery of the nondominant hand.

^{18}F -DMFP

^{18}F -DMFP was synthesized as described in detail previously (9). PET studies were performed on 16 healthy male volunteers with an age range of 24–44 y (mean \pm SD, 37 \pm 9 y). Subjects were positioned in a Siemens ECAT EXACT PET scanner so that the transaxial slices were parallel to the cantomeatal line, and the head was partially immobilized with elastic polystyrene straps. A 20-min-long transmission scan with an external ^{68}Ge ring source was acquired for attenuation correction of the emission recording. A 124-min-long dynamic emission recording in 3-dimensional (3D) mode consisting of 30 frames increasing in duration from 20 to 600 s was then initiated upon intravenous bolus injection of 209 \pm 50 MBq ^{18}F -DMFP (specific activity, 134–834 GBq/ μmol). Images were reconstructed in 47 planes with an interplane spacing of 3.375 mm, a matrix of 128 \times 128 voxels, and a final resolution (full width at half maximum [FWHM]) of 5.4 mm. Arterial radioactivity was recorded online during the first 10 min (ALLOGG AB blood sampler; Allogg Mariefred). Thereafter, samples were collected manually at 1-min intervals up to 20 min and then at 10-min intervals until the end of the recordings. After centrifugation, the plasma radioactivity was measured in a well counter cross-calibrated to the tomograph. Portions of plasma collected at 2, 5, 10, 20, 30, 40, 60, 90, and 120 min were analyzed for the fraction of

untransformed ^{18}F -DMFP using thin-layer chromatography (TLC) as described previously (9). The continuous unmetabolized radio-tracer input function was calculated by exponential fitting of the measured fractions (19).

^{18}F -FP

Chemistry. ^{18}F -FP was synthesized by a novel high-yield modification of the method for the synthesis of ^{18}F -DMFP (9). In brief, the tosylated precursor ((*S*)-*N*-[(1-allyl)-2-pyrrolidinyl]methyl]-5-(3-toluenesulfonyloxy-propyl)-2-methoxybenzamide (5 mg, 10 μmol) was dissolved in 1 mL acetonitrile, treated for 5 min at 65°C with potassium carbonate (5 mg, 36 μmol), and subsequently transferred into a 5-mL vial containing ^{18}F -fluoride using the method of Hamacher et al. (20). The reaction mixture was heated for 20 min at 85°C, diluted with 1 mL phosphoric acid (10%), and separated using high-performance liquid chromatography (HPLC) (250 \times 10 mm, RP8; CH_3CN : 0.25 mol/L ammonium acetate buffer + 5 mL acetic acid/L, 30:70; 5 mL/min). The fraction containing ^{18}F -FP was isolated, diluted with 0.15 mol/L disodium hydrogen phosphate buffer, and adsorbed on a C_{18} cartridge to remove the HPLC solvent. The column was washed with 2 mL water and the product was eluted with 1 mL ethanol. The eluant was diluted with 9 mL of an isotonic sodium chloride solution and sterilized by filtration (0.22 μm). Quality control before injection included determination of the chemical and radiochemical purity, specific activity, pH, and absence of pyrogens.

Scanning. Ten healthy male volunteers with an age range of 23–41 y (mean \pm SD, 32 \pm 9.5 y) were recruited for the study of ^{18}F -FP kinetics. After a 20-min transmission scan, a 240-min-long dynamic emission recording in 3D mode consisting of 45 frames increasing in duration from 20 to 600 s was initiated with the ECAT EXACT tomograph upon intravenous bolus injection of 184 \pm 43 MBq ^{18}F -FP (specific activity, 42–258 GBq/ μmol). Arterial blood sampling was as for ^{18}F -DMFP, with additional blood samples collected at 30-min intervals between 120 and 240 min. Metabolite correction was performed as for ^{18}F -DMFP.

^{11}C -RAC

Six healthy volunteers (4 males, 2 females) with an age range of 19–51 y (mean \pm SD, 33 \pm 11 y) were recruited for the study. A 90-min-long dynamic emission recording consisting of 20 frames increasing in duration from 30 to 300 s was recorded with the Scanditronics 4096+ tomograph in 2-dimensional (2D) mode after intravenous bolus injection of 745 \pm 18 MBq ^{11}C -RAC prepared by conventional methods (specific activity, 35–169 GBq/ μmol). After reconstruction, the final images had a spatial resolution of 6 \times 6 \times 6 mm FWHM with a matrix of 128 \times 128 voxels and 15 slices. A metabolite-corrected arterial input function was obtained as described previously (21).

Image Processing

All dynamic PET recordings were transferred to a Sun Workstation (Sun Microsystems) for further data analysis. Although great care was taken to minimize head movement, displacement (mainly in *z*-direction) was noted in some cases. Correction for this movement was accomplished as follows: Assuming no head movement during the first 10 min, the summed emission recording in this interval was manually resliced in the anterior commissure–posterior commissure orientation. All subsequent emission frames were realigned to this summed recording to optimize matching of the cerebral contours. To check for the quantity of misregistration, we applied a relatively large VOI in the striatum and the quality of

the final alignment was assessed framewise by visual inspection. Furthermore, striatal time–radioactivity curves (time–activity curve [TAC]) were extracted and evaluated for movement artifacts; if present, realignment was performed iteratively until no further improvement could be obtained. Final alignment was obtained by semiautomatic realignment of 30-min blocks of the emission sequence to the initial 10-min summed image. This was done semiautomatically, with manual adjustment where necessary, using commercially available software (MPI-Tool; ATV GmbH). The final dynamic emission recordings were summed and then automatically coregistered to the subject’s individual MRI scans.

VOIs drawn on the coregistered individual MR images were used to extract dynamic TACs from the caudate (circular), putamen (irregular), thalamus (elliptic), and cerebellum (irregular). These VOIs were defined in 3 adjacent transaxial slices passing through the regions of greatest extension of the 4 structures.

The magnitudes of V_d and BP in the VOIs were calculated by fitting several models to the time–radioactivity curves and, except where specified, parametric maps of V_d and BP were calculated from the entire dynamic emission recordings. Finally, the mean magnitudes of V_d and BP in the parametric maps were calculated for each anatomic VOI.

Kinetic Analyses

One- and 2-Tissue-Compartment Model. A 1-tissue-compartment, 3 parameter model with the plasma volume fixed at 0.05 mL g^{-1} (and using the whole blood radioactivity to calculate the contribution of vascular volume) was first fitted to the cerebellum TAC to determine the magnitude of V_d . Next, a 2-tissue-compartment, 5-parameter model, with the K_1/k_2 ratio constrained to the cerebellum observation V_d , was fitted to the time–radioactivity curves from the striatum and thalamus VOIs (9,18), and the BP was calculated as the ratio k_3/k_4 —that is the ratio of ligand association and dissociation rate constants.

Logan Plot with Arterial Input Function. The tracer V_d values in the VOIs were calculated by the linear graphical method of Logan et al. (13), and the magnitude of BP was calculated as the distribution volume ratio (DVR) relative to cerebellum, minus one. Voxelwise maps of BP were thus calculated using the commercially available software package PMOD (PMOD Technologies Ltd.) (22). Data recorded during the first 20 min were excluded from the linearizations.

Logan Plot with Reference Region. The magnitude of the DVR in the VOIs was calculated using the reference tissue linearization of Logan et al. (23), and the magnitude of BP was calculated as the DVR, minus one. Data recorded during the first 30 min were excluded from the linearizations. Voxelwise maps of BP were calculated using PMOD software.

Simplified Reference Region Compartmental Method (SRTM). The magnitude of BP was calculated in the VOIs using the simplified reference region (SRTM) compartmental method (11), and parametric maps of BP were made using the method of Gunn et al. (12), with the cerebellum serving as the reference region.

Linear Regression with Spatial Constraint Modified SRTM (LRSC). We have developed a modification of the SRTM for optimal calculation of parametric maps of BP by linear regression with spatial constraint (LRSC) (14). Applications of this method are generally based on an analytic solution of the SRTM equation with parameters estimated by multilinear regression. In this method, based on the same assumptions used to derive the SRTM, a new set of operational equations of integral form is derived with

parameters directly estimated by conventional weighted linear regression combined with general ridge regression with spatial constraints (24). The LRSC algorithm is implemented for parametric imaging to reduce the effects of high noise levels in voxelwise time–activity curves that are typical of dynamic PET data.

Simple Ratio. The simple ratio of specifically bound radioactivity in a receptor-containing (C_{RC}) and a receptor-free (C_{RF}) region, $(C_{RC} - C_{RF})/C_{RF}$, approaches the magnitude of BP at equilibrium. Using the VOIs, we calculated this ratio in the thalamus and striatum using the summed frames recorded during the interval 30–60 min in the case of ^{11}C -RAC, 60–90 min for ^{18}F -DMFP, and 150–180 min for ^{18}F -FP.

Statistics

To compare results of the different methods, Pearson correlation coefficients were calculated between the individual magnitudes for each ligand and brain region, using the commercial software package SPSS (SPSS Inc.). Significance was calculated after Fischer transformation.

RESULTS

Results of fitting the 2-tissue-compartment model and SRTM to representative time–radioactivity curves for ^{11}C -RAC, ^{18}F -DMFP, and ^{18}F -FP in the striatum (and cerebellum) are presented in Figure 1. Of the 3 tracers, ^{11}C -RAC and ^{18}F -DMFP clearly showed washout from the striatum during the 90- to 120-min-long recordings, whereas ^{18}F -FP appeared to reach a plateau in the striatum only after 180 min. Representative arterial input Logan plots for the 3 ligands in the striatum are shown in Figure 2. All 3 ligands appeared to have obtained a linear phase in the V_d plots within the recording intervals.

Although estimates of V_d and BP tended to be 5% higher in the putamen than in the caudate, there were no significant differences in the magnitudes of the estimates between these 2 tissues. Therefore, the results for the whole striatum—that is, the mean of the caudate and putamen—are presented. V_d

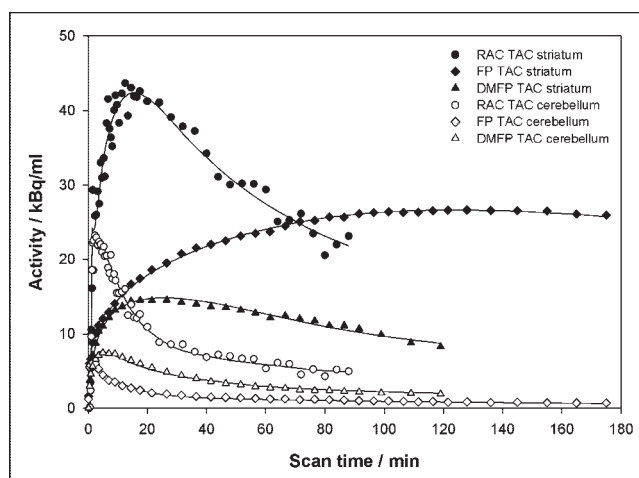


FIGURE 1. Plot of representative striatal TACs for ^{11}C -RAC, ^{18}F -DMFP, and ^{18}F -FP with fitted curves of simplified reference tissue model and corresponding cerebellar TACs with fitted curves of a 1-tissue-compartment model.

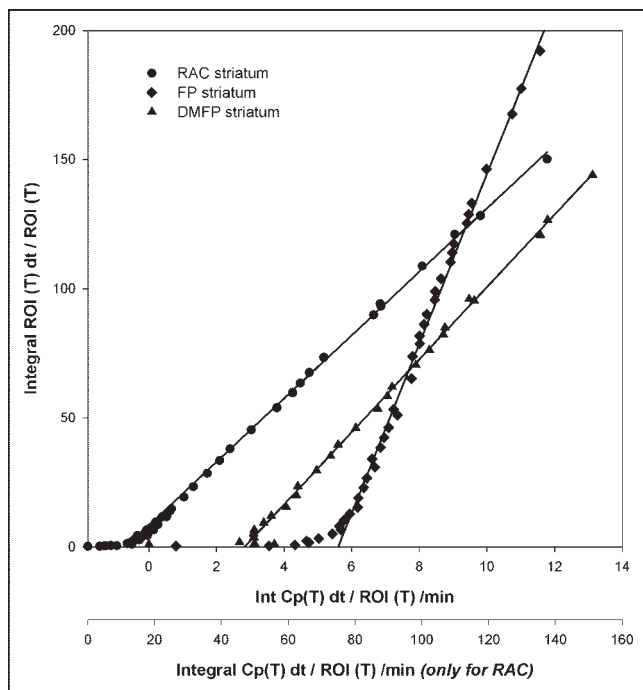


FIGURE 2. Plot of representative arterial Logan plots for ^{11}C -RAC, ^{18}F -DMFP, and ^{18}F -FP. ROI = region of interest; Int = integral.

values for the 3 ligands calculated using the constrained 2-tissue-compartment model with arterial input and the Logan arterial input method are summarized in Table 1. In the cerebellum, the rank order of V_d was ^{11}C -RAC < ^{18}F -FP <

^{18}F -DMFP. There were no significant differences in the magnitudes of the estimates by the 2 arterial input methods, nor were the coefficients of variation different. However, coefficients of variation were systematically lower in the case of ^{11}C -RAC (24%–42%) than for ^{18}F -FP and ^{18}F -DMFP (49%–70%).

Representative maps of BP calculated for the 3 ligands using the SRTM, the Logan arterial input plot, and the Logan reference tissue methods are presented in Figure 3. The results of the several methods for estimating BP in the thalamus and striatum in VOIs and voxelwise maps are summarized in Table 2. In the VOIs from the thalamus and striatum, the magnitude of BP calculated using the 2-tissue-compartment model tended to be 25% higher than that calculated by the other methods, except for ^{18}F -DMFP in the striatum, for which the coefficient of variation of the estimate was relatively high (30%). In both tissues, the rank order of BPs was ^{18}F -DMFP < ^{11}C -RAC < ^{18}F -FP; their magnitudes were approximately in the ratio 1:2:10 irrespective of the method of analysis. In the thalamus, the coefficients of variation of the mean voxelwise estimates of BP were generally less favorable for ^{18}F -DMFP (50%–58%) than for ^{11}C -RAC and ^{18}F -FP (10%–33%), irrespective of the method of analysis. The mean voxelwise estimates of BP in the VOIs were similar to the mean estimates for the whole VOI TACs. In the striatum, the coefficients of variation of the mean estimates of BP in the voxelwise maps were lower for ^{11}C -RAC (6%–8%) than for ^{18}F -DMFP or ^{18}F -FP (14%–20%).

TABLE 1

Summary of Equilibrium Distribution Volume (V_d , mL g^{-1}) for Benzamide Radioligands ^{18}F -DMFP, ^{11}C -RAC, and ^{18}F -FP Calculated Relative to Metabolite-Corrected Arterial Inputs by 2 Methods in Cerebellum, Thalamus, and Striatum of Healthy Control Subjects

V_d	Radiopharmaceutical	2-Tissue compartment	Comparison	Logan plot
Cerebellum	^{18}F -DMFP ($n = 16$)	3.87 ± 2.15	Voxel	3.43 ± 1.36
			VOI	3.00 ± 0.78
	^{11}C -RAC ($n = 6$)	0.35 ± 0.08	Voxel	0.38 ± 0.11
			VOI	0.39 ± 0.11
	^{18}F -FP ($n = 10$)	0.95 ± 0.53	Voxel	0.98 ± 0.47
			VOI	1.04 ± 0.53
Thalamus	^{18}F -DMFP	5.01 ± 3.52	Voxel	4.09 ± 1.57
			VOI	3.65 ± 0.80
	^{11}C -RAC	0.57 ± 0.15	Voxel	0.56 ± 0.18
			VOI	0.58 ± 0.16
	^{18}F -FP	3.34 ± 1.87	Voxel	3.07 ± 1.99
			VOI	2.92 ± 1.53
Striatum	^{18}F -DMFP	12.19 ± 7.14	Voxel	11.05 ± 5.01
			VOI	9.54 ± 2.18
	^{11}C -RAC	1.79 ± 0.76	Voxel	1.58 ± 0.46
			VOI	1.64 ± 0.51
	^{18}F -FP	30.24 ± 19.45	Voxel	27.23 ± 18.88
			VOI	32.67 ± 20.62

Each estimate is mean \pm SD of 16 separate determinations in the case of ^{18}F -DMFP, 6 in the case of ^{11}C -RAC, and 10 in the case of ^{18}F -FP.

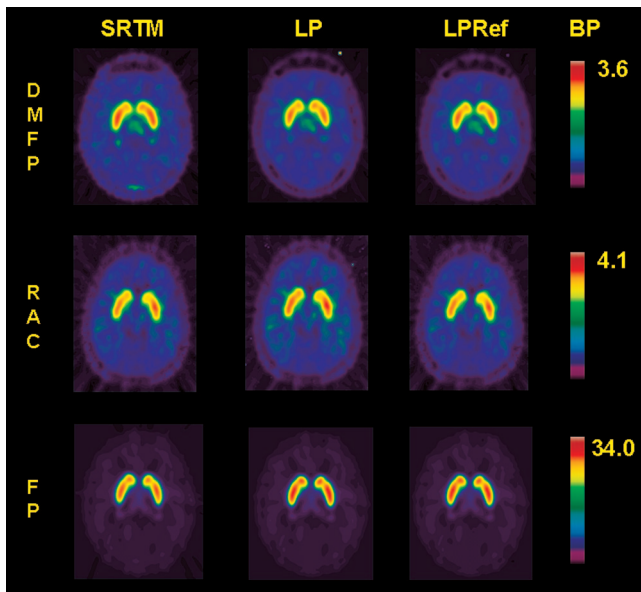


FIGURE 3. Representative parametric maps of BP of ^{18}F -DMFP, ^{11}C -RAC, and ^{18}F -FP calculated by simplified reference tissue method SRTM (left column), arterial input Logan plot LP (middle column), and reference tissue Logan plot LPRef (right column).

Estimates of specific ^{18}F -FP binding by the simple ratio (measured 150–180 min after injection) gave values close to the calculated BP for ^{18}F -FP in the striatum but overestimated thalamic binding. Simple ratios for ^{11}C -RAC and ^{18}F -DMFP yielded higher values for the striatum and extrastriatal binding than did the BP calculations. The variance for the simple ratio was of similar magnitude for all tracers compared with the BP estimates.

The results of correlation analysis of the several methods are presented in Table 3. In general, the several estimates of ^{11}C -RAC BPs correlated less well with each other than did those for ^{18}F -DMFP and ^{18}F -FP. The standard 2-tissue-compartment arterial input model BPs correlated significantly with results from the Logan arterial input method only for the case of ^{18}F -DMFP. However, the 2-tissue-compartment BPs correlated significantly with SRTM BPs for all 3 ligands. Highest correlations for all 3 ligands were between the SRTM and Logan cerebellum input methods.

DISCUSSION

The majority of PET studies of dopamine $D_{2/3}$ receptors so far have been accomplished using the radiopharmaceutical ^{11}C -RAC. However, the short physical half-life of ^{11}C precludes its use at imaging centers without an on-site medical cyclotron. The present study was intended to compare the sensitivities of ^{11}C -RAC with 2 relatively novel ^{18}F -labeled benzamides, which we routinely synthesize using ^{18}F obtained from other institutions. To this end, the binding of 3 benzamide radioligands for dopamine $D_{2/3}$ receptors was assessed in normal human brain by parametric mapping analysis and VOI analysis and using arterial input and reference tissue methods. In analogy to other methodologic publications (25,26), this comparison was solely based on groups of healthy volunteers, who are assumed to consist of a single homogeneous population. For practical reasons, we could not obtain recordings for the 3 tracers in the same subject group. All 3 ligands have high selectivity for dopamine $D_{2/3}$ receptors, but they are quite distinct with respect to their affinities.

Whereas the apparent in vivo affinity of ^{18}F -DMFP for $D_{2/3}$ receptors (15 nmol/L) is close to that of ^{11}C -RAC (26

TABLE 2
Summary of BPs for Benzamide Radioligands ^{18}F -DMFP, ^{11}C -RAC, and ^{18}F -FP in Thalamus and Entire Striatum Calculated Using Several Metabolite-Corrected Arterial Input Models and Reference Tissue Models

BP	Comparison	Thalamus			Striatum		
		^{18}F -DMFP	^{11}C -RAC	^{18}F -FP	^{18}F -DMFP	^{11}C -RAC	^{18}F -FP
2-Tissue compartment	VOI	0.26 ± 0.15	0.62 ± 0.09	3.27 ± 1.16	1.93 ± 0.58	4.00 ± 0.84	34.45 ± 5.87
Logan plot arterial	Voxel	0.20 ± 0.10	0.46 ± 0.13	2.26 ± 0.53	2.20 ± 0.37	3.12 ± 0.25	26.60 ± 5.27
	VOI	0.23 ± 0.12	0.47 ± 0.08	1.96 ± 0.54	2.21 ± 0.32	3.16 ± 0.19	26.32 ± 5.72
Logan plot cerebellum	Voxel	0.21 ± 0.11	0.40 ± 0.13	2.11 ± 0.51	2.20 ± 0.35	3.02 ± 0.19	23.68 ± 4.81
	VOI	0.24 ± 0.13	0.47 ± 0.07	1.88 ± 0.53	2.19 ± 0.31	3.14 ± 0.20	23.03 ± 4.80
SRTM	Voxel	0.22 ± 0.11	0.49 ± 0.13	2.17 ± 0.45	2.35 ± 0.36	3.16 ± 0.21	21.72 ± 4.10
	VOI	0.24 ± 0.11	0.43 ± 0.13	1.90 ± 0.55	2.29 ± 0.32	3.17 ± 0.21	23.26 ± 4.89
LRSC	Voxel	0.31 ± 0.17	0.51 ± 0.05	2.23 ± 0.51	2.47 ± 0.34	3.26 ± 0.23	22.49 ± 4.04
Simple ratio	Voxel	1.21 ± 0.13	1.50 ± 0.08	3.83 ± 1.08	3.74 ± 0.54	5.10 ± 0.38	30.06 ± 7.47

First, a 2-tissue compartment model was fitted to TACs in VOIs defined for thalamus and striatum. An arterial input Logan analysis, reference tissue Logan analysis, conventional simplified reference tissue method (SRTM), and SRTM with linear regression and spatial constraint (LRSC) were likewise used to calculate BPs in time-radioactivity curves from thalamus and striatum VOIs; in addition, mean voxelwise estimates in parametric maps were calculated for the same VOIs. Finally, the simple ratios of VOI activity to cerebellum activity at steady state are reported. Each estimate is mean \pm SD of 16 separate determinations in the case of ^{18}F -DMFP, 6 in the case of ^{11}C -RAC, and 10 in the case of ^{18}F -FP.

TABLE 3
Spearman Correlation Coefficients for Estimation of BP in Striatum for Tracers ^{18}F -DMFP, ^{11}C -RAC, and ^{18}F -FP

	Radiopharmaceutical	2-Tissue compartment	Logan plot arterial input	Logan cerebellum input	SRTM	LRSC	Simple ratio
2-Tissue compartment	^{18}F -DMFP		0.80*	0.70*	0.56†	0.40	0.46
	^{11}C -RAC	1	-0.25	0.78	0.91†	0.41	0.40
	^{18}F -FP		0.85	0.94†	0.95†	0.54	0.28
Logan arterial input	^{18}F -DMFP			0.91*	0.81*	0.52†	0.59‡
	^{11}C -RAC		1	0.36	0.13	0.30	0.52
	^{18}F -FP			0.56	0.59	0.51	0.60
Logan plot cerebellum	^{18}F -DMFP				0.89*	0.51†	0.78*
	^{11}C -RAC			1	0.96*	0.75	0.65
	^{18}F -FP				0.99*	0.98*	0.90*
SRTM	^{18}F -DMFP					0.66‡	0.70*
	^{11}C -RAC				1	0.68	0.64
	^{18}F -FP					0.96*	0.88*
LRSC	^{18}F -DMFP						0.39
	^{11}C -RAC					1	0.39
	^{18}F -FP						0.86*
Simple ratio	^{18}F -DMFP						
	^{11}C -RAC						1
	^{18}F -FP						

BP was calculated using a 2-tissue compartment model and Logan method using metabolite-corrected arterial inputs and by Logan reference tissue method, conventional simplified reference tissue method (SRTM), and SRTM with linear regression and spatial constraint (LRSC). Also, the simple ratio of striatum to cerebellum at equilibrium was calculated. Significance of interclass correlations by method: † $P < 0.05$, ‡ $P < 0.01$, * $P < 0.005$, calculated for 16 subjects in the case of ^{18}F -DMFP, 6 subjects in the case of ^{11}C -RAC, and 10 in the case of ^{18}F -FP.

nmol/L) (27), the relatively novel compound ^{18}F -FP has substantially higher affinity (33 pmol/L) than the other 2 benzamides in the present study (28–30). This high affinity provides the basis for the particular sensitivity of ^{18}F -FP for the detection of extrastriatal $D_{2/3}$ receptors (Fig. 3). However, this same high affinity of ^{18}F -FP imposes a requirement for lengthy emission recordings to obtain an equilibrium binding estimate in the striatum.

In addition to their differing affinities for the dopamine $D_{2/3}$ receptors, the present 3 benzamides are distinct with respect to their nonspecific binding in the cerebellum. Whereas ^{11}C -RAC has a relatively low V_d in the cerebellum, that of ^{18}F -FP was 2-fold higher and that of ^{18}F -DMFP was 10-fold higher. Given the structural similarities and similar log P values (30) of these benzamides, we cannot readily account for the 10-fold difference in the V_d but suggest that additional factors, such as the (unmeasured) plasma protein binding, may account for the high V_d of ^{18}F -DMFP. The high variance in the calculation of the V_d for ^{18}F -DMFP and ^{18}F -FP in the cerebellum and striatum might conceivably be attributed to imprecision in the calculation of the metabolite-corrected arterial input, especially at late times when the concentration of untransformed tracer in plasma is vanishingly small. However, using TLC, we were able to obtain adequate metabolite correction throughout the emission recordings for all 3 tracers.

In general, high nonspecific binding reduces the signal-to-noise ratio in the calculation of specific binding. Thus,

the superior precision of the estimates of ^{11}C -RAC BP in the thalamus and striatum may be attributed in part to its low nonspecific binding. This phenomenon may also contribute to the poor sensitivity of ^{18}F -DMFP for the detection of dopamine receptors in the thalamus, where they are not abundant. However, the pharmacologic specificity of the ^{11}C -RAC binding detected in the thalamus has not been demonstrated in previous displacement studies or pharmacologic challenge studies, although we have reported a partial displacement of N - ^{11}C -methylspiperone binding in pig thalamus by methylenedioxymethamphetamine challenge (7). The ratio of BP in the striatum to that in the thalamus is much higher for ^{18}F -FP (12:1) than for ^{11}C -RAC (6:1) irrespective of the method of analysis, suggesting that thalamic binding may be overestimated using the latter tracer.

In the striatum, where dopamine receptors are most abundant, the trade-off between precision and accuracy in the estimation of BP is different than that in the thalamus; the coefficient of variation of the BP in the striatum was somewhat less favorable for ^{18}F -FP than for ^{18}F -DMFP, in spite of the former compound's lower nonspecific binding. Here, the very slow approach to equilibrium binding for ^{18}F -FP may compromise the precision of the estimate of its BP in the striatum, even given the present 4-h-long emission recordings.

Irrespective of the method used for parametric mapping, the BP for ^{11}C -RAC was in the range 3–4 in normal human

striatum, as reported previously by others in VOIs using bolus infusion (11,31,32) or continuous infusion methods (26). The SRTM approach for quantifying ^{11}C -RAC binding was validated by Gunn et al. (12). In the present study, we likewise find substantial agreement between the estimates obtained in parametric maps and in striatal VOIs for the case of SRTM and other models. This suggests that the present use of voxelwise mapping does not bias the estimation of the magnitude of the ^{11}C -RAC BP in the striatum. However, the 2-tissue-compartment model gave higher BP estimates than did the other models, albeit with a penalty in precision in the cases of ^{11}C -RAC and ^{18}F -DMFP. Although a relatively high BP for ^{11}C -RAC based on the 2-compartment model has been noted previously (7), overspecification of this model may compromise the precision of the estimate of BP. Thus, on the basis of the present results, we conclude that SRTM presents optimal properties for the generation of parametric maps with ^{11}C -RAC, based on the high correlation between SRTM results and the gold standard of the 2-tissue-compartment model. It has earlier been argued that the spatial constraint approach yields lower image noise in BP maps and is, therefore, preferable to SRTM for accurate stereotactic normalization (14). In the present study, the spatial constraint approach gave slightly (5%) higher BPs for ^{11}C -RAC. The performance of SRTM is dependent on the noise level of kinetics; as noise levels decrease, results calculated by the LRSC approach those obtained by SRTM and the Logan plot with reference region input. SRTM and the Logan plot can have higher noise-induced bias (usually underestimation), but this bias is minimized by LRSC or BP estimates (14).

In the present study, the cerebral kinetics of ^{18}F -DMFP binding have been evaluated in a large number of healthy volunteers ($n = 16$). As in an earlier report on only 10 subjects (9), there was considerable agreement between several arterial input and reference tissue methods for the calculation of BP. However, as discussed, the precision of the estimate in the striatum was lower than that for the other 2 ligands tested in the present study—a difference that we attribute to the high nonspecific binding of ^{18}F -DMFP. Given the similar in vitro affinities reported for ^{11}C -RAC and ^{18}F -DMFP, it is unclear why ^{18}F -DMFP had a lower BP than ^{11}C -RAC did in the present study of living human brain, confirming earlier studies on rhesus monkeys (8). The BP of ^{18}F -DMFP may be underestimated because of its high nonspecific binding relative to the other tracers, which, we speculate, could be related to difference in plasma protein binding since the log P values are quite similar (30). We have found ^{18}F -DMFP and the SPECT ligand iodobenzamide to be equally suitable for the discrimination of idiopathic and atypical parkinsonian syndromes using a simple ratio method (33). Though, on the basis of the present results, ^{18}F -DMFP may not be superior to ^{11}C -RAC for the estimation of availability of dopamine $\text{D}_{2/3}$ receptors in the striatum, we have argued that it presents a potential practical advantage due to the greater transportability of ^{18}F . Further-

more, ^{18}F -DMFP may present an advantage over ^{11}C -RAC in the single bolus or continuous infusion competition paradigms (34,35). The occurrence of a prolonged equilibrium for ^{18}F -DMFP binding in the striatum compared with ^{11}C -RAC predicts that the effects of pharmacologic challenge on dopamine release in the striatum might sensitively be detected in the course of an ^{18}F -DMFP recording of several hours' duration. This advantage may outweigh the higher radiation burden imposed by ^{18}F -DMFP (effective dose equivalent: ^{11}C -RAC, 0.01 mSv/MBq; ^{18}F -DMFP, 0.03 mSv/MBq; ^{18}F -FP, 0.017 mSv/MBq). However, the present findings suggest that ^{18}F -DMFP is particularly unsuited for the detection of extrastriatal dopamine receptors.

Depending on the method used for analysis, in the present study we found ^{18}F -FP to have a BP of 21–32 in human striatum, as reported previously by Mukherjee et al. (30). The 2-tissue-compartment model BPs correlated significantly with the Logan reference tissue results and with the 2 SRTM results. Therefore, we conclude that arterial inputs are not necessary for good quantitation of the ^{18}F -FP BP in human striatum. In contrast to ^{11}C -RAC and ^{18}F -DMFP (9,11), it might be that not all criteria for estimation of BP by reference tissue methods are fulfilled by ^{18}F -FP (e.g., $k_2 > k_4$). Nevertheless, in our group of subjects, the Logan plots were always linear during the time interval used for analysis, which tends to validate the use of these equilibrium methods. Furthermore, the reference tissue Logan plot has been used for ^{18}F -FP quantitation in several previous publications (e.g., 30).

The present estimates of the BP of ^{18}F -FP in the thalamus (2.0–2.8) were somewhat lower than those in an earlier report (30). Diverse methodologic differences, especially related to the method for drawing the VOI, or in the selection of the frames to which the linearization was applied may be responsible for this difference.

Simple ratio techniques for receptor quantitation are suited to the requirements of clinical investigations, where patients cannot remain in the tomograph for extended periods. Therefore, we tested the correlation between the simple ratio relative to cerebellum measured during a 30-min static recording and several BP estimates. This correlation was not significant for ^{11}C -RAC in the striatum but was significant in the case of several estimates obtained by voxelwise methods for ^{18}F -FP and ^{18}F -DMFP. This phenomenon may be related to the superior signal available from ^{18}F . However, the ratio method overestimated the BP of ^{18}F -DMFP and ^{11}C -RAC in the thalamus and, to a lesser extent, also in the striatum. Since the time required to reach equilibrium is dependent on receptor density, the simple ratio measured at an optimal time point for striatal binding need not perfectly reflect the BP in regions with lower D_2 receptor density (36). Thus, the performance of the simple ratio method is dependent on the chosen time frame. Furthermore, differences in the magnitude of K_1 (the unidirectional clearance from vascular space to brain tissue) on the estimation of BP may also contribute to the bias from this simple method

(34). Thus, the present ratio approach seems inadequate for assessing dopamine D_{2/3} receptor availability in brain regions with different receptor densities.

The practical necessity of using different subject groups in the present comparison of 3 different ligands imposes some limitations on the interpretations to be drawn from the study. However, since there was no statistically significant difference in age ($P > 0.05$) between the groups, a confound due to age can be excluded, especially since the declines in BP with increasing age are, in any event, relatively small (8% per decade) (37,38). Nevertheless, some of the present intergroup differences could reflect individual differences in competition from endogenous dopamine at the time of scanning.

Intrinsic differences in binding parameters between study groups may contribute to the higher variability in ¹⁸F-DMFP and ¹⁸F-FP binding between subjects compared with ¹¹C-RAC. Intrasubject variability (i.e., test–retest) has been reported to be 5% for ¹¹C-RAC (37) and 10% for ¹⁸F-FP (30), suggesting that the binding of the latter ligand may be intrinsically more variable in a normal population. Alternately, steady-state ¹⁸F-FP binding estimates may be more difficult to measure due to the slow approach to its equilibrium. To our knowledge, the present study constitutes the first report on intersubject variability in ¹⁸F-DMFP binding, indicating a somewhat higher intrasubject variability than is typical for ¹¹C-RAC. Intrinsic variability may be a factor in selecting a probe for the sensitive detection of differences in clinical populations and under conditions of pharmacologic activation studies.

One limitation of the present study is that ¹¹C-RAC data were acquired in 2D mode using a different tomograph than that used for testing the new ligands, ¹⁸F-DMFP and ¹⁸F-FP. Nonetheless, the present estimates of ¹¹C-RAC binding are very similar to previous estimates in healthy subjects (15) obtained using a tomograph (ECAT 931) with a performance similar to that of the present instrument used for ¹⁸F-DMFP and ¹⁸F-FP acquisitions. Since the resolution of the PC4096+ (39) is comparable to that of the ECAT EXACT (40), we conclude that the potential bias introduced by instrumentation is not a major factor in the present comparison of the 3 ligands.

CONCLUSION

Voxelwise maps of the BP of ¹¹C-RAC, ¹⁸F-DMFP, and ¹⁸F-FP were generated in the brains of groups of healthy volunteers. The magnitudes of the estimates of BP obtained by arterial input methods and reference tissue methods were generally well correlated in the striatum. Adequate quantitation of thalamic BP could be obtained with ¹⁸F-FP and ¹¹C-RAC but not ¹⁸F-DMFP, possibly due to the high non-specific binding of the latter tracer. In general, there was close agreement between several estimates of the BP obtained in voxelwise maps by VOI analysis. In summary, the Logan plot, SRTM, and LRSC methods are reliable and

robust methods for the parametric mapping of ¹⁸F-DMFP and ¹¹C-RAC binding. Although the very high affinity of ¹⁸F-FP predicts a slow approach to equilibrium binding in the striatum, our results suggest that the Logan plot and SRTM method provide stable estimates of the BP. Furthermore, simple binding ratios for ¹⁸F-FP (striatum/cerebellum) measured in the 150- to 180-min interval gave values close to the BP in the striatum, although this interval was not optimal for the assessment of extrastriatal binding.

ACKNOWLEDGMENTS

This study was partially supported by the Deutsche Forschungsgemeinschaft (grant Ba 1011/2-1). We thank Sabine Hoehnemann and Stephan Maus for the preparation of radiopharmaceuticals ¹⁸F-DMFP and ¹⁸F-FP and Heike Armbrust-Henrich for her help with data acquisition.

REFERENCES

- Brooks DJ, Ibanez V, Playford ED, et al. Presynaptic and postsynaptic striatal dopaminergic function in neuroacanthocytosis: a positron emission tomographic study. *Ann Neurol*. 1991;30:166–171.
- Farde L, Suhara T, Nyberg S, et al. A PET-study of [¹¹C]FLB 457 binding to extrastriatal D₂-like dopamine receptors in healthy subjects and antipsychotic drug-treated patients. *Psychopharmacology*. 1997;133:396–404.
- Vernaleken I, Siessmeier T, Buchholz H-G, et al. High striatal occupancy of D₂-like dopamine receptors by amisulpride in brain of patients with schizophrenia. *Int J Neuropsychopharmacol*. 2004;7:421–430.
- Heinz A, Siessmeier T, Wrase J, et al. Nucleus accumbens dopamine D₂ receptors correlate with central processing of alcohol cues and craving. *Am J Psychiatry*. 2004;161:1783–1789.
- Farde L, Ehrin E, Eriksson L, et al. Substituted benzamides as ligands for visualization of dopamine receptor binding in the human brain by positron emission tomography. *Proc Natl Acad Sci USA*. 1985;82:3863–3867.
- Kohler C, Hall H, Ogren SO, Gawell L. Specific in vitro and in vivo binding of ³H-raclopride: a potent substituted benzamide drug with high affinity for dopamine D-2 receptors in the rat brain. *Biochem Pharmacol*. 1985;34:2251–2259.
- Rosa-Neto P, Gjedde A, Olsen AK, et al. MDMA-evoked changes in [¹¹C]raclopride and [¹¹C]NMSP binding in living pig brain. *Synapse*. 2004;53:222–233.
- Mukherjee J, Yang ZY, Brown T, Roemer J, Cooper M. ¹⁸F-Desmethoxyfallypride: a fluorine-18 labeled radiotracer with properties similar to carbon-11 raclopride for PET imaging studies of dopamine D₂ receptors. *Life Sci*. 1996;59:669–678.
- Gründer G, Siessmeier T, Piel M, et al. Quantification of D₂-dopamine receptors in the human brain with ¹⁸F-desmethoxyfallypride [published correction appears in *J Nucl Med*. 2003;44:145]. *J Nucl Med*. 2003;44:109–116.
- Mukherjee J, Yang ZY, Lew R, et al. Evaluation of d-amphetamine effects on the binding of dopamine D-2 receptor radioligand, ¹⁸F-fallypride in nonhuman primates using positron emission tomography. *Synapse*. 1997;27:1–13.
- Lammertsma AA, Hume SP. Simplified reference tissue model for PET receptor studies. *Neuroimage*. 1996;4:153–158.
- Gunn RN, Lammertsma AA, Hume SP, Cunningham VJ. Parametric imaging of ligand-receptor binding in PET using a simplified reference region model. *Neuroimage*. 1997;6:279–287.
- Logan J, Fowler JS, Volkow ND, et al. Graphical analysis of reversible radioligand binding from time-activity measurements applied to [¹¹C-methyl]-(-)-cocaine PET studies in human subjects. *J Cereb Blood Flow Metab*. 1990;10:740–747.
- Zhou Y, Endres CJ, Brasic JR, Huang SC, Wong DF. Linear regression with spatial constraint to generate parametric images of ligand-receptor dynamic PET studies with a simplified reference tissue model. *Neuroimage*. 2003;18:975–989.
- Lammertsma AA, Bench CJ, Hume SP, et al. Comparison of methods for analysis of clinical [¹¹C]raclopride studies. *J Cereb Blood Flow Metab*. 1996;16:42–52.
- Koepp MJ, Gunn RN, Lawrence AD, et al. Evidence for striatal dopamine release during a video game. *Nature*. 1998;393:266–268.
- Zubieta JK, Smith YR, Bueller JA, et al. Regional mu opioid receptor regulation of sensory and affective dimensions of pain. *Science*. 2001;293:311–315.
- Koepp RA, Holthoff VA, Frey KA, Kilbourn MR, Kuhl DE. Compartmental analysis of [¹¹C]flumazenil kinetics for the estimation of ligand transport rate and

- receptor distribution using positron emission tomography. *J Cereb Blood Flow Metab.* 1991;11:735–744.
19. Gillings NM, Bender D, Falborg L, Marthi K, Munk OL, Cumming P. Kinetics of the metabolism of four PET radioligands in living minipigs. *Nucl Med Biol.* 2001;28:97–104.
 20. Hamacher K, Coenen HH, Stoecklin G. Efficient stereospecific synthesis of 2-[¹⁸F]-fluoro-2-deoxy-D-glucose using aminopolyether supported nucleophilic substitution. *J Nucl Med.* 1986;27:235–238.
 21. Cumming P, Yokoi F, Chen A, et al. Pharmacokinetics of radiotracers in human plasma during positron emission tomography. *Synapse.* 1999;34:124–134.
 22. Burger C, Mikolajczyk K, Grodzki M, Rudnicki P, Szabatin M, Buck A. JAVA tools quantitative post-processing of brain PET data [abstract]. *J Nucl Med.* 1998;39(suppl):277P.
 23. Logan J, Fowler JS, Volkow ND, Wang GJ, DingYS, Alexoff DL. Distribution volume ratios without blood sampling from graphical analysis of PET data. *J Cereb Blood Flow Metab.* 1996;16:834–840.
 24. Zhou Y, Huang SC, Bergsneider M, Wong DF. Improved parametric image generation using spatial-temporal analysis of dynamic PET studies. *Neuroimage.* 2002;15:697–707.
 25. Lassen NA, Bartenstein PA, Lammertsma AA, et al. Benzodiazepine receptor quantification in vivo in humans using [¹¹C]flumazenil and PET: application of the steady-state principle. *J Cereb Blood Flow Metab.* 1995;15:152–165.
 26. Ito H, Hietala J, Blomqvist G, Halldin C, Farde L. Comparison of the transient equilibrium and continuous infusion method for quantitative PET analysis of [¹¹C]raclopride binding. *J Cereb Blood Flow Metab.* 1998;18:941–950.
 27. Ehrin E, Farde L, de Paulis T, et al. Preparation of ¹¹C-labelled raclopride, a new potent dopamine receptor antagonist: preliminary PET studies of cerebral dopamine receptors in the monkey. *Int J Appl Radiat Isot.* 1985;36:269–273.
 28. Mukherjee J, Yang ZY, Das MK, Brown T. Fluorinated benzamide neuroleptics. III. Development of (S)-N-[(1-allyl-2-pyrrolidinyl)methyl]-5-(3-[¹⁸F]fluoropropyl)-2,3-dimethoxybenzamide as an improved dopamine D-2 receptor tracer. *Nucl Med Biol.* 1995;22:283–296.
 29. Mukherjee J, Yang ZY, Brown T, et al. Preliminary assessment of extrastriatal dopamine D-2 receptor binding in the rodent and nonhuman primate brains using the high affinity radioligand, ¹⁸F-fallypride. *Nucl Med Biol.* 1999;26:519–527.
 30. Mukherjee J, Christian BT, Dunigan KA, et al. Brain imaging of ¹⁸F-fallypride in normal volunteers: blood analysis, distribution, test-retest studies, and preliminary assessment of sensitivity to aging effects on dopamine D-2/D-3 receptors. *Synapse.* 2002;46:170–188.
 31. Wang GJ, Volkow ND, Fowler JS, et al. Reproducibility of repeated measures of endogenous dopamine competition with [¹¹C]raclopride in the human brain in response to methylphenidate. *J Nucl Med.* 1999;40:1285–1291.
 32. Hietala J, Nagren K, Lehtikoinen P, Ruotsalainen U, Syvalahti E. Measurement of striatal D2 dopamine receptor density and affinity with [¹¹C]-raclopride in vivo: a test-retest analysis. *J Cereb Blood Flow Metab.* 1999;19:210–217.
 33. Schreckenberger M, Hägele S, Siessmeier T, et al. The dopamine D2-receptor ligand F-18 desmethoxyfallypride is an appropriate PET tracer for the differential diagnosis of parkinsonism. *Eur J Nucl Med Mol Imaging.* 2004;31:1128–1135.
 34. Endres CJ, Carson RE. Assessment of dynamic neurotransmitter changes with bolus or infusion delivery of neuroreceptor ligands. *J Cereb Blood Flow Metab.* 1998;18:1196–1210.
 35. Watabe H, Endres CJ, Breier A, Schmall B, Eckelman WC, Carson RE. Measurement of dopamine release with continuous infusion of [¹¹C]raclopride: optimization and signal-to-noise considerations. *J Nucl Med.* 2000;41:522–530.
 36. Olsson H, Farde L. Potentials and pitfalls using high affinity radioligands in PET and SPET determinations on regional drug induced D2 receptor occupancy: a simulation study based on experimental data. *Neuroimage.* 2001;14:936–945.
 37. Volkow ND, Wang GJ, Fowler JS, et al. Measuring age-related changes in dopamine D2 receptors with ¹¹C-raclopride and ¹⁸F-N-methylspiroperidol. *Psychiatry Res.* 1996;67:11–16.
 38. Inoue M, Suhara T, Sudo Y, et al. Age-related reduction of extrastriatal dopamine D2 receptor measured by PET. *Life Sci.* 2001;69:1079–1084.
 39. Rota Kops E, Herzog H, Schmid A, Holte S, Feinendegen LE. Performance characteristics of an eight-ring whole body PET scanner. *J Comput Assist Tomogr.* 1990;14:437–445.
 40. Wienhard K, Eriksson L, Grootenck S, Casey M, Pietrzyk U, Heiss WD. Performance evaluation of the positron scanner ECAT EXACT. *J Comput Assist Tomogr.* 1992;16:804–813.

